IOPscience iopscience.iop.org

Home Search Collections Journals About Contact us My IOPscience

Coalescence and movement of nanobubbles studied with tapping mode AFM and tip–bubble interaction analysis

This article has been downloaded from IOPscience. Please scroll down to see the full text article.

2008 J. Phys.: Condens. Matter 20 485004

(http://iopscience.iop.org/0953-8984/20/48/485004)

View the table of contents for this issue, or go to the journal homepage for more

Download details:
IP Address: 129.252.86.83
The article was downloaded on 29/05/2010 at 16:40

Please note that terms and conditions apply.

J. Phys.: Condens. Matter **20** (2008) 485004 (10pp) doi:10.1088/0953-8984/20/48/485004

Coalescence and movement of nanobubbles studied with tapping mode AFM and tip–bubble interaction analysis

Bharat Bhushan[1,4], **Yuliang Wang**[1,2] **and Abdelhamid Maali**[3]

[1] Nanoprobe Laboratory for Bio- & Nanotechnology and Biomimetics (NLB[2]), The Ohio State University, 201 West 19th Avenue, Columbus, OH 43210-1142, USA
[2] Mechanical Engineering, Harbin Institute of Technology, Harbin 150001, People's Republic of China
[3] Centre de Physique Moleculaire Optique et Hertzienne, University Bordeaux I, 351 cours de la Liberation, F-33405 Talence, France

E-mail: Bhushan.2@osu.edu

Received 14 July 2008, in final form 5 September 2008
Published 17 October 2008
Online at stacks.iop.org/JPhysCM/20/485004

Abstract
Imaging of a polystyrene (PS) coated silicon wafer immersed in deionized (DI) water was conducted using atomic force microscopy (AFM) in the tapping mode (TMAFM). As reported earlier, spherical cap-like domains, referred to as nanobubbles, were observed to be distributed on the PS surface. Experiments reveal that, in addition to the well-known parameter of scan load, scan speed is also an important parameter which affects nanobubble coalescence. The process of nanobubble coalescence was studied. It was found that during coalescence, small nanobubbles were easily moved and merged into bigger ones. Based on the interaction between the AFM cantilever tip and a bubble in the so-called force modulation mode of TMAFM, bubble height and adhesive force information for a given bubble was extracted. A viscoelastic model is used to obtain the interaction stiffness and damping coefficient, which provides a method to obtain the mechanical properties of nanobubbles. The model was further used to study the effect of surface tension force on attractive interaction force and contact angle hysteresis on the changes of the interaction damping coefficient during tip–bubble interaction.

(Some figures in this article are in colour only in the electronic version)

1. Introduction

Interactions between hydrophobic surfaces and aqueous solutions have been extensively studied over past decades, using various techniques to probe static and dynamic behavior. During wetting of a hydrophobic surface with a polar solvent (e.g. water), spherical cap bubbles with dimensions of 5–100 nm in height and 0.1–0.8 μm in diameter are produced (Ishida *et al* 2000, Lou *et al* 2000, Tyrrell and Attard 2002, Holmberg *et al* 2003, Simonsen *et al* 2004, Zhang *et al* 2006). These bubbles with nanoscale dimensions are generally called nanobubbles. The study of nanobubbles during liquid flow in micro/nanochannels is of interest in micro/nanofluidics based biosensors (Bhushan 2007). Theoretical studies (Watts *et al* 1990, Lauga and Stone 2003, Cottin-Bizonne *et al* 2004, Sbragaglia and Prosperetti 2007) and experimental studies (Ou *et al* 2004, Joseph *et al* 2006) suggest that at the liquid–solid interface, the presence of nanobubbles is responsible for the apparent slip or, more specifically, the breakdown of the no-slip condition for hydrophobic surfaces. To reduce pressure drop and volume loss in micro/nanochannels, it is desirable to minimize drag and increase slip at the liquid–solid boundary. It has also been reported that nanobubbles can act as an anti-lubricant and promote high friction (Steinberger *et al* 2007). Additionally, the measured long-range (10–100 nm) attractive forces on the hydrophobic surfaces using TMAFM are believed to be due to the presence of nanobubbles. According to Ishida *et al* (2002), the coalescence of bubbles on hydrophobic surfaces is believed

[4] Author to whom any correspondence should be addressed.

 © 2008 IOP Publishing Ltd Printed in the UK

to form a gas bridge and lead to the long-range attractive force. The existence of nanobubbles has been detected by various techniques, such as AFM, rapid cryofixation/freeze fracture (Switkes and Ruberti 2004) and neutron reflectometry (Steitz *et al* 2003). Molecular dynamics (MD) simulations have also been used to explain the existence of nanobubbles (Koishi *et al* 2004). AFM has become a powerful tool for morphological characterization and force detection on the molecular scale. Holmberg *et al* (2003) have used contact mode AFM and argued that it can be used to image nanobubbles even though the tip penetrates the surface of the bubble, which may compromise the image quality. In tapping mode AFM, an oscillating tip intermittently contacts the sample surface with much lighter force exerted on the sample than contact mode AFM (Zhong *et al* 1993, Tamayo and Garcia 1996, Bar *et al* 1998, Bhushan 2008). Thus, the technique is widely used to detect soft and fragile materials. Several researchers have tried to image nanobubbles in the tapping mode (Ishida *et al* 2000, Lou *et al* 2000, Tyrrell and Attard 2002, Yang *et al* 2003, Simonsen *et al* 2004, Agrawal *et al* 2005, Zhang *et al* 2006).

The bubbles generally appear to be quite stable and long-lived, with lifetimes over 20 h (Attard 2003, Yang *et al* 2003). In TMAFM, nanobubbles can be coalesced, and the larger bubbles are generated by applying a high load (Yang *et al* 2003, Simonsen *et al* 2004). For AFM tip–bubble interaction, the typical force–distance curve from force calibration mode AFM is obtained in an area containing nanobubbles (Ishida *et al* 2002, Holmberg *et al* 2003, Steitz *et al* 2003).

Although the existence of nanobubbles has been confirmed by imaging and bubble coalescence has been observed, the detailed process of nanobubble coalescence is not understood. Moreover, viscoelastic properties should be explored for tip–bubble interaction in addition to the force–distance curves between AFM tip and bubble. With an oscillating tip interacting with an object in TMAFM, one can extract the mechanical properties of the object with amplitude and phase shift information (Aime *et al* 2001, Jeffery *et al* 2004, Maali *et al* 2006a).

In this study, we first imaged nanobubbles on a PS coated silicon surface by using liquid TMAFM with a modified liquid cell. By applying higher load or lower scan speed, movement and coalescence of nanobubbles were observed. Further evidence of coalescence was given by calculating the quantity of gas molecules trapped in the selected nanobubbles. Furthermore, a viscoelastic tip–bubble interaction model was used to calculate the interaction stiffness and damping coefficient between AFM tip and nanobubbles. The model was further used to study the effect of surface tension on attractive interaction force and contact angle hysteresis on the changes in the interaction damping coefficient during tip–bubble interaction.

2. Experimental details

In the general operation of liquid AFM, the whole liquid cell is excited by a piezoelectric element, which results in a multitude of spurious peaks related to the fluid cell eigenfrequencies. Therefore, it is difficult to clearly determine the resonance frequencies of the cantilever. In this paper, a modified tip holder (Maali *et al* 2006b) was used to directly provide piezo-excitation to the cantilever in fluid with a commercial MultiMode III AFM in the tapping mode (digital instruments), as shown in figure 1. A horizontal slot was carved out in the opening of the commercially available tip holder for non-fluid use above the piezo-element in order to insert a glass slide. When the liquid is added between the glass slide and the substrate, a liquid meniscus is formed between the glass and sample surface for fluid imaging.

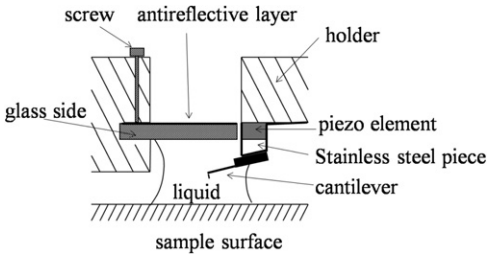

Figure 1. Schematic diagram of the modified tip holder.

A silicon cantilever RFESP (rotated force-modulated etched silicon probe, Digital Instruments) with a tip radius <10 nm and a stiffness of 3 N m^{-1} quoted by the manufacturer was used. The measured resonance frequencies in air and water were about 73.6 and 25.9 KHz, respectively. While imaging in air and liquid, we chose the drive frequencies close to the cantilever resonance frequency. A scan rate of 2 Hz with a 90° scan angle was used for imaging.

All experiments were performed in a controlled ambient environment (temperature: $22 \pm 1\,^{\circ}$C), and the liquid imaging was conducted in deionized (DI) water. The sample surface was first imaged in air by TMAFM, then the sample was immersed into DI water to perform liquid imaging. The free oscillation amplitude of the cantilever at working frequency was 7.0 nm. An amplitude of 6.65 nm (namely 95% of free amplitude) was chosen for bubble imaging. An amplitude of 6.30 nm (90% of free amplitude) to apply higher load was chosen for coalescence. The same region of 5 μm $\times$ 5 μm scan area was selected for all images shown in this paper. To compare consequences of bubble coalescence and movement, a central 2 μm $\times$ 2 μm scan area was generally selected to perform higher load scans. Then imaging was carried out in the 5 μm $\times$ 5 μm scan area with a 95% setpoint to check corresponding changes. The choice of the 95% setpoint for checking changes is important to avoid any unexpected change to nanobubbles.

Additionally, a so-called auto ramp function combined with force modulation mode was used in TMAFM to get a series of curves of amplitude and phase shift as a function of distance over a certain area in the liquid. In the auto ramp function, the piezotube performs a vertical extension and retraction movement relative to the tapping cantilever tip along the x and y axes separately with a fixed step, and the cantilever driving frequency and amplitude remains constant. Piezotube vertical frequency was chosen as 1 Hz, and vertical extension was 200 nm during auto ramping. A step of 30 nm was chosen along both x and y axes on about 1 μm $\times$ 1 μm scan area which

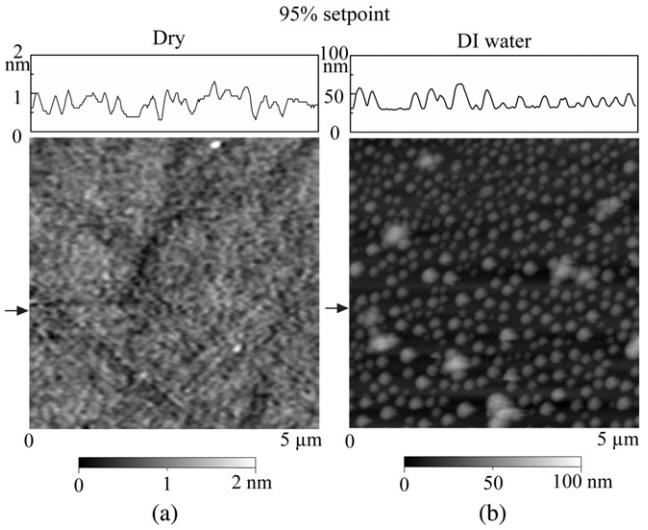

Figure 2. Comparison of images of PS coated silicon wafer using tapping mode AFM in (a) air and (b) DI water.

contains a bubble. At each test location on the nanobubble, curves of amplitude and phase as a function of distance were obtained.

A polystyrene (PS) surface for nanobubble imaging used in the study was prepared by the spin coating method on a silicon (100) wafer. The polystyrene particles (molecular weight 350 000, Sigma-Aldrich) were dissolved in toluene (Mallinckrodt Chemical) with a concentration of about 0.23 mg ml^{-1}, and the speed for spin coating was 500 rpm. The contact angle of the PS surface obtained with the sessile drop method was $95° \pm 3°$, which shows that the sample surface is hydrophobic.

3. Results and discussions

3.1. Imaging of nanobubbles

By performing TMAFM in air, a featureless image of the original PS coated silicon wafer surface is obtained, as shown in figure 2(a). The roughness $\boldsymbol{\sigma}$ and peak to valley distances R_{max} are 0.21 nm and 2.3 nm, respectively. Figure 2(b) shows the image of the PS surface immersed in DI water. The entire surface is covered with spherical cap-like domains. The diameter and height of these caps are generally of the order of 200 nm and 20 nm, respectively. The values of roughness $\boldsymbol{\sigma}$ and R_{max} are 8.2 nm and 68.7 nm, respectively, which are about two orders of magnitude larger than that obtained in air. Some big domains are observed in the vicinity where the bubbles' distribution density is lower than in other places. That may be because of local bubble coalescence.

3.1.1. Influence factors during nanobubble imaging. The PS sample in water over the same 5 μm × 5 μm area was scanned for several hours. The measurements show that nanobubbles are stable except when the scan parameters were changed. It is well known that nanobubbles can coalesce together by increasing the scan load (Steitz *et al* 2003, Simonsen *et al* 2004).

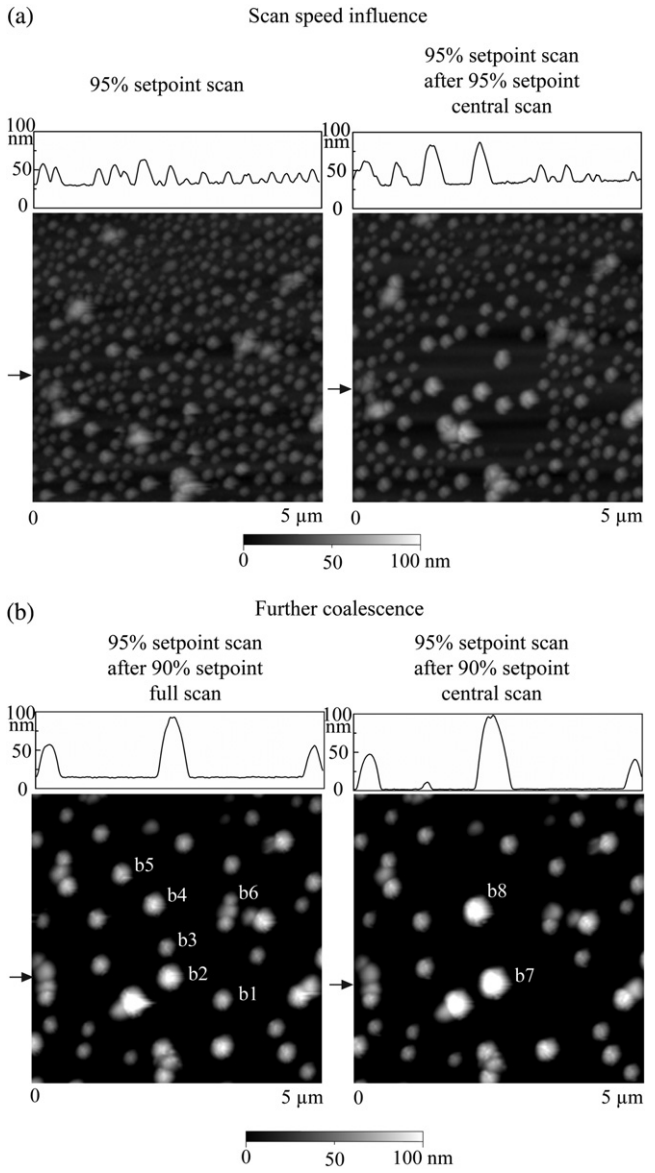

Figure 3. Sequence of nanobubble images obtained in the same 5 μm × 5 μm scan area with (a) 95% amplitude setpoint scan (left); 95% amplitude setpoint scan preceded by scanning with 95% amplitude setpoint in the central 2 μm × 2 μm area repeated twice (right). Nanobubble coalescence is observed with lower scan speed in the central area. (b) 95% amplitude setpoint scan preceded by scanning with 90% amplitude setpoint in the full 5 μm × 5 μm scan area (left); and 95% amplitude setpoint scan preceded by scanning with 90% amplitude setpoint in the central 2 μm × 2 μm area repeated twice (right). Further coalescence of nanobubbles is observed.

Here we find that the scan speed can also affect nanobubble imaging.

Figure 3(a) (left) was obtained at 95% setpoint and full 5 μm × 5 μm area scan. Then the central 2 μm × 2 μm area scan was performed twice with the same 95% amplitude setpoint. After that, we went back to scan a 5 μm × 5 μm area with 95% setpoint and got the image shown in figure 3(a) (right). We can find bigger bubbles generated in the central area with lower distribution density. The diameter and height

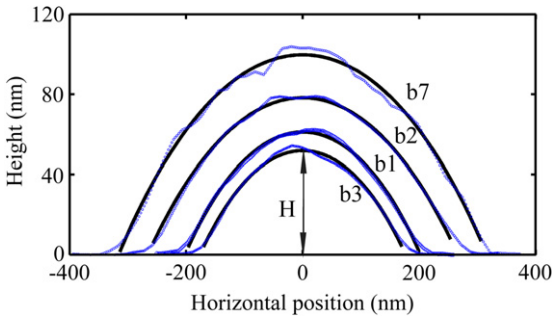

Figure 4. Cross section profiles of bubbles b1, b2, b3 and b7 in figure 3(b) through the apex of bubbles. The solid curves correspond to the least-square-fit curves by fitting the profiles as circular arcs. H is the height of bubbles shown in table 1.

Table 1. Height H_i and fitted radius of curvature R_i for bubbles b1, b2, b3 and b7 marked in figure 3(b) (left and right) and the corresponding inside pressure p_i, volume V_i and the value $p_i \times V_i$. The calculation of inside pressure is based on the Laplace–Young equation of equation (1) and the volume of nanobubbles is obtained through the values of H_i and R_i by treating nanobubbles as spherical caps.

Bubble	Height H_i (nm)	Radius R_i (nm)	Pressure p_i (atm)	Volume V_i ($\times 10^6$ nm^3)	$p_i \times V_i$ ($\times 10^{-6}$ nNm)
b1	51.8	325.6	5.4	2.6	1.4
b2	78.2	490.9	3.9	8.9	3.5
b3	61.1	364.7	4.0	4.0	2.0
b7	99.7	550.3	3.6	16.2	5.9

of nanobubbles increase to 420 nm and 55 nm from 200 nm and 20 nm, respectively, in figure 3(a). Therefore, some bubbles must coalesce and generate bigger ones. The only difference between the 2 μm$\times$2 μm central area scan of figure 3(a) (right) and figure 3(a) (left) is the scan speed. When working at the same scan rate, the scan speed in the 5 μm $\times$ 5 μm area scan is one-and-a-half times higher than that in the 2 μm $\times$ 2 μm area scan. Assuming the power transferred from the cantilever tip to sample surfaces is constant during a certain period of time, the low scan speed implies higher power transfer for the same scan area than for high scan speed, and nanobubbles suffer more disturbance. Therefore, the coalescence occurred even with the same setpoint of amplitude.

From the above experiment, one can find that nanobubbles are very sensitive to scan parameters while imaging. In addition to scan load, scan speed can also affect nanobubble imaging. To get original nanobubble images without movement and coalescence, a higher setpoint (corresponding to lower scan load), higher scan rate and larger scan area are desirable. If the scan parameters are not chosen properly, the bubbles will be coalesced or moved during imaging, and in some cases cannot be observed.

3.1.2. Process of nanobubble coalescence. As mentioned in section 1, although the nanobubble coalescence has been observed, the detailed process is not understood. Additionally, it is still not clear whether nanobubbles will dissolve into solution or merge together with perturbation of the cantilever tip while imaging. Here we explore the detailed process of nanobubble coalescence in nanobubble images. Moreover, the coalescence is verified through a calculation based on conservation of the number of gas molecules before and after nanobubble coalescence, as shown in figure 3(b).

After applying 90% setpoint scan in the whole 5 μm $\times$ 5 μm area of figure 3(a) (right), a 95% setpoint scan was performed in the full area and nanobubble images with a lower distribution density were obtained, as shown in figure 3(b) (left). Nanobubble distribution density is reduced while the bubble size abruptly increases with the normal diameter over 550 nm and height over 77 nm. With lower bubble distribution density in figure 3(b) (left), it is possible to track certain bubbles' coalescence. In the central area containing six numbered bubbles of figure 3(b) (left), the central 2 μm$\times$2 μm area scan was performed twice with 90% setpoint. After that, a 95% setpoint scan was performed over the full area, and a further nanobubble coalescence image was obtained, as shown in figure 3(b) (right), where the diameter and height of nanobubbles increase from 550 nm and 77 nm up to 690 nm and 100, respectively.

By comparing figure 3(b) (left) with figure 3(b) (right), one can find that, except for the six numbered bubbles in figure 3(b) (left), the sizes and locations of other bubbles remained unchanged in figure 3(b) (right). Based on their locations, we believe that the bubbles b1, b2 and b3 coalesced together and generated the bigger bubble b7. Similarly, b4, b5 and b6 join together to generate bubble b8. More importantly, one can find that during nanobubble coalescence, small bubbles (b1, b3 and b5, b6) tend to move first and coalesce with b2 and b4, generating bigger bubbles. This should be because the big bubbles have strong interaction with the surface due to their long length of contact line with the surface.

To verify nanobubble coalescence, the quantity of gas molecules trapped in nanobubbles before and after coalescence is calculated. We assume the total number of gas molecules trapped into nanobubbles before and after coalescence remains constant. According to the Laplace–Young equation (Israelachvili 1992, Bhushan 1999, 2002):

$$\Delta p = 2\gamma/R, \tag{1}$$

where R is the radius of a spherical bubble, γ is surface tension ($\gamma = 72$ mN m^{-1} for water) of the liquid, and Δp is the pressure difference between the inside and outside of the spherical bubble, the inside pressure of nanobubbles should change during coalescence. Because the bubble b6 is close to another bubble and the diameter measurement is not accurate, here we take the group of nanobubbles b1, b2, b3 and b7 for example. Figure 4 shows the section profiles through the apex of the bubbles and the corresponding fitted curve of nanobubbles b1, b2, b3 and b7 in figure 3(b). $p_i \times V_i$ is used to evaluate the quantity of gas molecules in the nanobubbles, where p_i and V_i are inside pressure and volume of the bubble i, respectively. With the height and radius of the fitted curves shown in figure 4, the volume and the term $p_i \times V_i$ for the bubbles b1, b2, b3 and b7 are obtained, as shown in table 1.

The result shows that $p_{b7} \times V_{b7} = 5.9 \times 10^{-6}$ nNm, which is smaller than $p_{b1} \times V_{b1} + p_{b2} \times V_{b2} + p_{b3} \times V_{b3} =$

6.9×10^{-6} nNm of the bubbles b1, b2 and b3. Note here a difference of 14.5% of the quantity $p_i \times V_i$ before and after coalescence. This occurs because of uncertainties in the value of the measured volume and also because of the gas dissolution during bubble movement and coalescence. Since nanobubbles are highly deformable and easily penetrated during imaging, the height of nanobubbles during imaging should be underestimated (Vinckier *et al* 1996, Chen *et al* 1998, Zhang *et al* 2006). According to the Laplace–Young equation, the pressure in big bubbles is smaller than that in small ones. The influence of height underestimation should be bigger for big bubbles than small ones for their much softer properties. In summary, there should be less than 14.5% of the gas dissolved into water during this process.

3.2. Tip–bubble interaction analysis

To study tip–bubble interaction, experiments were conducted in the force modulation mode using TMAFM in a 1 μm $\times$ 1 μm area scan containing bubble b7 in figure 3(b) (right). Figure 5 shows the amplitude and phase shift as a function of separation distance between cantilever and substrate on the bubble and bare substrate. The amplitude was calibrated using the slope of amplitude—piezotube displacement while the tip approaches or retracts relative to the substrate. The phase shift at large tip–substrate separation is treated as $-90°$. From figure 5(a), one can clearly see the difference in amplitude response as a function of separation distance with and without the bubble. In the extending curve on the bubble, the amplitude exhibited an abrupt decrease (snap-in) from the free oscillation. Once tip and bubble came into contact, the oscillation amplitude gradually decreased due to interaction between the cantilever and the bubble. Therefore, the distance D_{height} can be regarded as the height of the bubble. Similar measurements of actual bubble heights have been reported with force calibration curves (Holmberg *et al* 2003). In the retracting curve on the bubble, the piezotube pulls the sample away from the tip. The oscillation amplitude gradually increases with increasing separation distance between tip and sample surface and has the same trend as with the extending curve at the beginning stage. However, the tip does not lose contact with the bubble at the corresponding snap-in of the extending curve, which is because of an adhesive force between cantilever tip and the bubble. Therefore, the distance D_{ad} is related to the adhesive force between the cantilever tip and the bubble in a monotonic manner. In both the extension and retraction curves on the substrate, no difference is observed.

Figure 5(b) shows the phase shift signal of the cantilever as a function of tip–substrate separation distance. When the cantilever approaches the sample surface, the phase shift signal first decreases with a decrease in the separation distance, and then gradually increases. During the initial stage of tip–bubble interaction, the attractive force is present and decreases with a further decrease of separation force. It is this attractive force which is responsible for variation in the phase shift (Garcia and San Paulo 1999).

By performing force modulation experiments over a bubble, experimental results show a clear trend of variation for

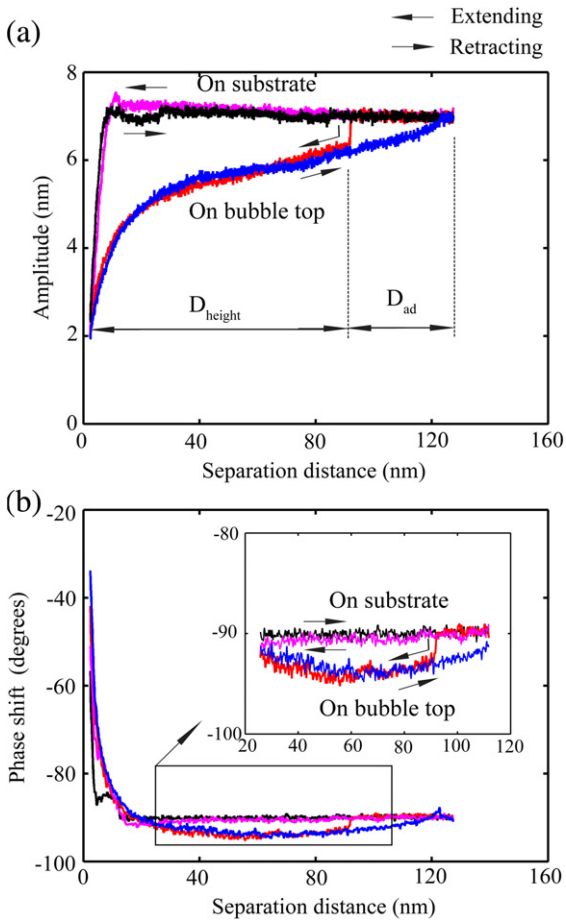

Figure 5. (a) Amplitude and (b) phase shift as a function of separation distance during extension and retraction modes with a tapping cantilever tip on the PS substrate and a coalesced bubble labeled b7 in figure 3(b) (right). The amplitude gradually decreases with decreasing separation distance for the bubble as compared with that on the PS substrate, while the phase shift first decreases and then increases.

the value D_{height} and D_{ad}, as shown in figures 6(b) and (c). Six curves are selected from the data taken at 16 points along a randomly selected scan line in auto ramp function, as shown in figure 6(a). The exact locations of these six curves are marked in figure 6(b). For curve 1, one can expect that the tip is on the edge of the bubble. That is because the extending curve is just like that on the substrate while the retracting curve is typical of on-bubble response, similar to the retraction curve on the bubble in figure 5(a). From curve 2 to curve 5, the tip extends and retracts along the profile of the bubble until curve 6, where the tip interacts with the substrate, and on-bubble response is not observed. One should note that for all the curves, the tip encountered hard contact with substrate surface at the same location where the amplitude drops down to a value close to zero. This is evidence to distinguish a nanobubble from contamination particles during nanobubble imaging. According to the force modulation curve, we believe that the cantilever tip penetrates the nanobubble and the solid–liquid–gas contact line moves upward along the tip axis during the process of tip–bubble interaction in force modulation mode.

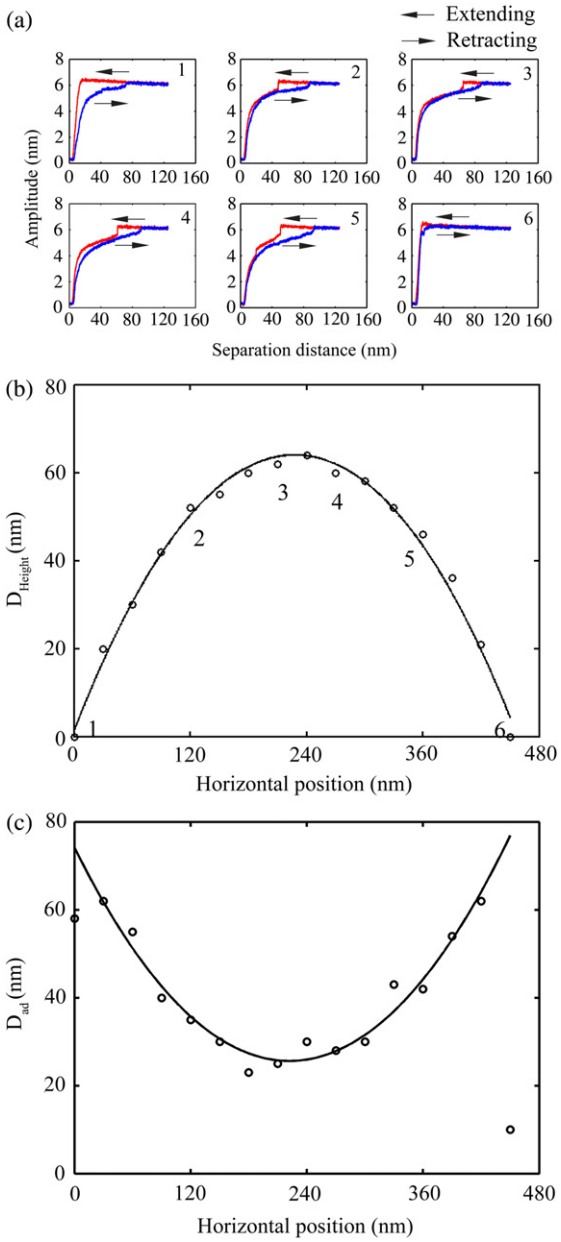

Figure 6. (a) Selected six curves (corresponding to points 1–6 in (b)) of amplitude as a function of separation distance along a scan line of a coalesced bubble labeled b7 in figure 3(b) (right). At locations 1–3, height of bubble increases and at locations 4–6, height of bubble decreases. (b) Height of bubble (D_{height}) as a function of horizontal position along the scan line. The value first increases and then decreases following the profile of the bubble. (c) The distance D_{ad} with respect to each point of (b). The value D_{ad} decreases with increasing height of bubble (D_{height}) along the scan line and vice versa.

Two trends can be observed from tip–bubble interaction curves. One is that D_{height} first increases and then decreases following the profile of the bubble, as shown in figure 6(b). The other observation is that the trend of D_{ad} with horizontal position is inversely related to D_{height}. It is clear that D_{ad} reaches its minimum value around the apex of the bubble profile. At the edge of the bubble, D_{ad} is large. The inverse relationship between D_{ad} and D_{height} is believed to be due to the

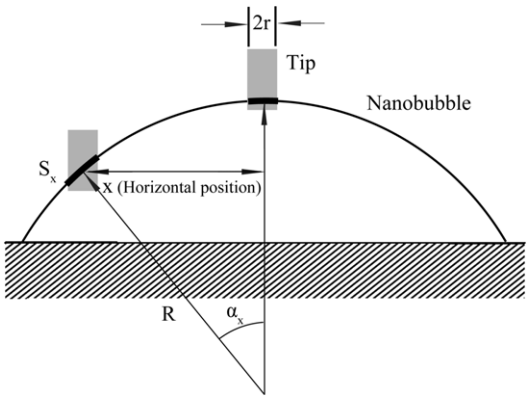

Figure 7. Schematic diagram of a simplified cylindrical tip and the nanobubble at different positions of the nanobubble. In the figure, r is the radius of a cylindrical tip, R is the radius of the nanobubble, S_x is the perimeter of the contact area. The perimeter of the contact area at the edge is larger than that close to the apex of the nanobubble.

variation of the length of the contact line between the cantilever tip and the bubble at different positions of the nanobubble. When tip–bubble interaction occurs at the edge of the bubble, a large area of the side of the tip will contact with the bubble. The total length of the contact line is expected to be larger than that on the apex of the bubble due to the profile and small radius of the cantilever tip. Hence, the adhesive force on the edge is larger than that on the apex of the bubble. To simply explain the influence of interaction position on D_{ad}, a schematic diagram of tip–bubble interaction is given in figure 7. In the figure, the cantilever tip is treated as a cylindrical tip with radius r, and the radius of the nanobubble is R. The diameter of the contact line at the apex of the nanobubble can be simply regarded as the diameter of the cylindrical tip. When the cylindrical tip is in contact with the bubble at the position x relative to the axis of the spherical cap, the radius of the contact area can be approximately treated as $r/\cos\alpha_x$, where α_x is the central angle at the position x. Therefore, the diameter of the contact area at the position x can be given as $r_x \approx r/\sqrt{1-\sin^2\alpha_x} = r/\sqrt{1-(x/R)^2}$. The adhesion force F_{ad} which is due to capillary force from a capillary bridge during retracting movement of the cantilever tip is proportional to the perimeter S_x of the contact area, and hence the diameter r_x, $F_{ad} \propto r_x$. Meanwhile, the value D_{ad} is proportional to the adhesive force F_{ad}. Therefore, the relationship $D_{ad} \propto r_x$ is satisfied. From the expression of r_x, one can find that the contact line increases with the increasing value of x (horizontal position), which indicates that the adhesion force increases when the tip approaches the edge of the nanobubble.

To study tip–bubble interaction, in this paper, a viscoelastic model is used. In the model, the interaction between the bubble and cantilever can be viewed as a nonlinear spring, of which interaction stiffness k_{int} and damping coefficient c_{int} are tip–bubble distance dependent, as shown in figure 8. k_c and c_0 are the stiffness and damping coefficients of the cantilever. During tip–bubble interaction, the total stiffness k_{tot} and damping coefficient c_{tot} are given as

$$k_{tot} = k_c + k_{int}, \tag{2}$$

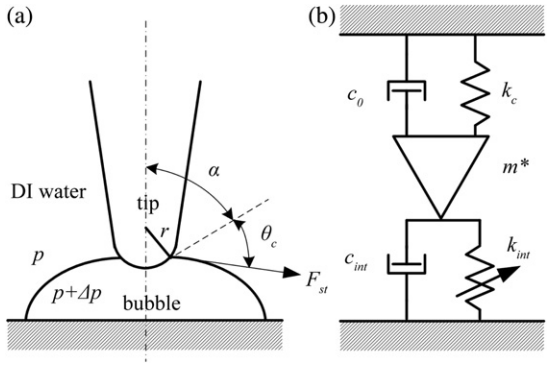

Figure 8. (a) Schematic diagram of interaction between cantilever tip and bubble and (b) equivalent viscoelastic model for tip–bubble interaction analysis.

and

$$c_{\text{tot}} = c_0 + c_{\text{int}}. \tag{3}$$

Motion of the cantilever can be viewed as a damped driven harmonic oscillator (Bhushan 2008). For a cantilever oscillating with a small amplitude, the force induced by the interaction of the tip with the liquid has two contributions: the conservative term ($-k_{\text{int}}z$) and the dissipative term ($-c_{\text{int}}\dot{Z}$). The well-known vibration equation for an oscillating cantilever is given as (Paulo and Garcia 2002, Jeffery *et al* 2004, Maali *et al* 2006a),

$$m^*\ddot{z} + c_{\text{tot}}\dot{z} + k_{\text{tot}}z = F_0 \exp(\text{i}\omega t), \tag{4}$$

where z and m^* are the instantaneous position and effective mass of the cantilever, ω is the driving frequency and $F_0 = k_{\text{c}}A_0/Q$ is the driving force, in which Q and A_0 are the quality factor and free oscillation amplitude, respectively. The damping coefficient of the cantilever far from the substrate surface is related to the quality factor Q ($Q \sim 5$ in this case) and the resonance frequency ω_0 via the equation $c_0 = m^*\omega_0/Q = \frac{k_{\text{c}}}{\omega_0 Q}$, which is calculated as 3.6×10^{-6} N m^{-1} s. The stationary solution $z = A\exp\text{i}(\omega t + \varphi)$ of equation (4) gives the interaction stiffness and damping coefficient (Maali *et al* 2006a)

$$k_{\text{int}} = k_{\text{c}}\left(\frac{A_0\cos(\varphi)}{AQ} - 1 + \frac{\omega^2}{\omega_0^2}\right), \tag{5}$$

and

$$c_{\text{int}} = -c_0\left(\frac{\omega_0 A_0}{\omega A}\sin(\varphi) + 1\right), \tag{6}$$

where A and φ are measured amplitude and phase shift, respectively. The cantilever was operated close to its resonance frequency, as mentioned in the experimental section, hence the term ω/ω_0 is close to 1. Equations (5) and (6) can be rewritten as

$$k_{\text{int}} = k_{\text{c}}\frac{A_0\cos(\varphi)}{AQ}, \tag{7}$$

and

$$c_{\text{int}} = -c_0\left(\frac{A_0}{A}\sin(\varphi) + 1\right). \tag{8}$$

By utilizing the amplitude and phase shift data presented in figure 5, we obtain the interaction stiffness and damping coefficient as a function of separation distance for the extension and retraction movement of the piezotube on the bubble and substrate, as shown in figure 9.

During extension movement on the bubble, the value of interaction stiffness changes rapidly, corresponding to the change in amplitude at the snap-in point of figure 5(a). The interaction stiffness is smaller than that on the substrate at the same separation distance. That means that there is an attractive force between the cantilever tip and the bubble. The magnitude of the attractive force first increases with decreasing separation distance and then gradually decreases until the attractive force diminishes and the repulsive force dominates the interaction. This trend is consistent with the results reported based on the force–distance curve in force calibration mode AFM by Ishida *et al* (2000) and Holmberg *et al* (2003), and their results also show that attractive force dominates the range of tip–bubble interaction.

We believe the attractive force present during tip–bubble interaction is due to the surface tension force present at the tip–water–gas interface. During advancing and receding of a particle in a bubble or a droplet, the contact angle at the tip–water–air contact line during the advancing process is different from that of the receding process (Scheludko and Nikolov 1975, Ecke *et al* 1999, Tao and Bhushan 2006). In this study, we assume the contact angle at the tip–water–air interface follows its wetting properties when the tip extends and retracts relative to the bubble. As shown in figure 8, θ_{c} is the contact angle, α is the tip cone angle at the contact line where the tip penetrates the bubble, and r is the tip radius. F_{st} is the surface tension force acting around the contact line and satisfies $F_{\text{st}} = 2\gamma\pi r\cos\alpha$. Therefore, the total interaction force (F_{int}) along the vertical direction between cantilever tip and bubble can be given as:

$$F_{\text{int}} = F_{\text{st}}\cos(\alpha + \theta_{\text{c}}) + \Delta p\pi\,(r\cos\alpha)^2 \tag{9}$$

where Δp is the Laplace pressure given by equation (1). From equation (9), one can find that, when $\alpha + \theta_{\text{c}} > 90°$, the direction of surface tension force is downward; otherwise, it is upward. If $F_{\text{int}} < 0$, the interaction force (F_{int}) will be attractive to the cantilever tip. The interaction stiffnesses shown in figures 9(a) and (c) demonstrate that the $F_{\text{int}} < 0$ condition is satisfied during tip–bubble interaction (about 80 nm for extension mode and 100 nm for retraction mode). Similar to the amplitude response, the interaction stiffness on the bubble is smaller than that on the substrate for the retraction curve at the snap-in, which means the surface tension force still dominates the interaction until the tip finally loses contact with the bubble.

When it comes to the interaction damping coefficient, we can clearly see the difference between the values for bubble and substrate. The damping coefficient on the substrate remains unchanged from the separation distance 130–10 nm for both extension and retraction curves, whereas the damping coefficient on the bubble gradually increases with decreasing separation distance. Because the height of the cantilever tip we used in the experiment is about 17.5 μm and comparable to the cantilever width, the influence of hydrodynamic force due

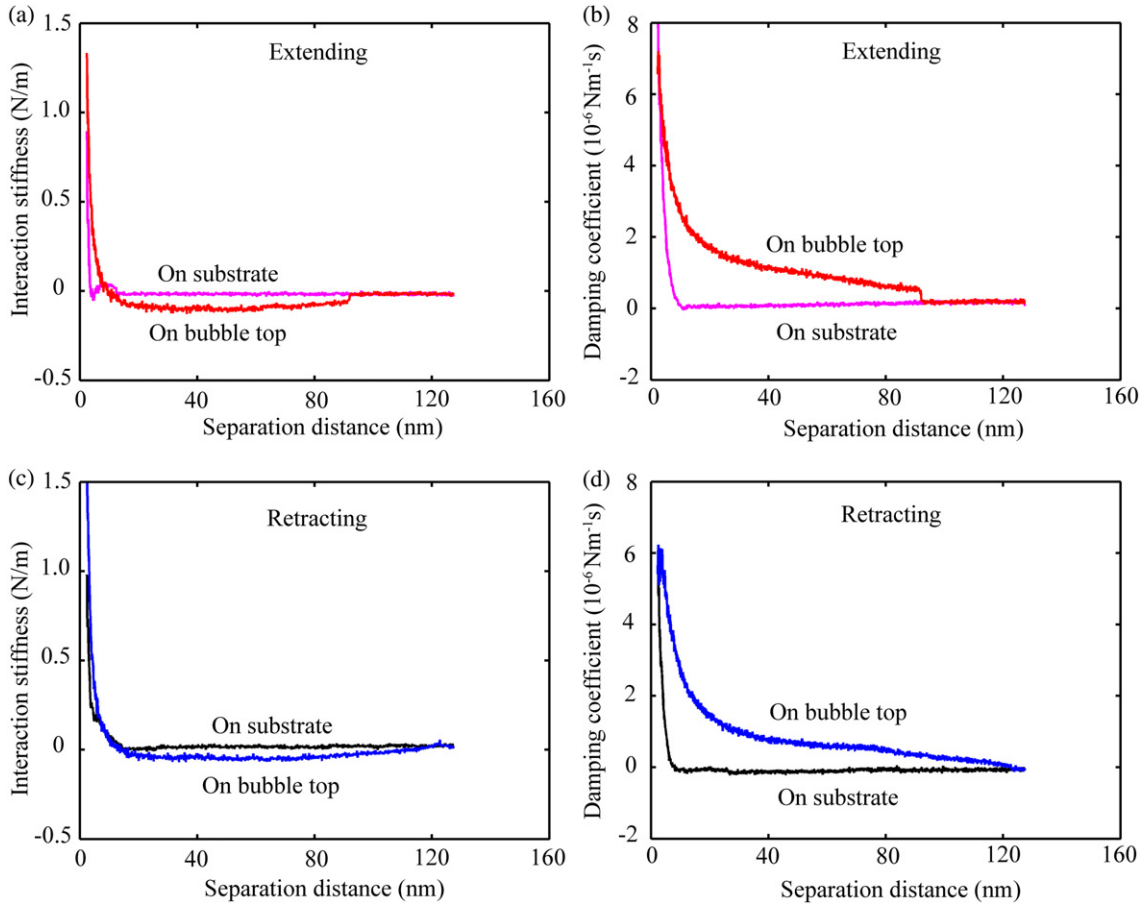

Figure 9. Comparison of interaction stiffness during (a) extension and (c) retraction modes, and interaction damping coefficient during (b) extension and (d) retraction modes as a function of separation distance between cantilever tip and sample surface on the PS substrate and the top of the coalesced bubble labeled b7 in figure 3(b) (right). It shows a long range of attractive tip–bubble interaction and increasing damping coefficient with decreasing separation distance between tapping cantilever tip and sample substrate comparing with that on the substrate.

to squeezed water can be neglected (Vinogradova *et al* 2001), which explains the observation of no change in the damping coefficient on the substrate until the separation distance is less than about 10 nm. However, on nanobubbles, damping coefficient increases with a decrease in the separation distance. Because the data on the substrate shows a negligible effect of the squeezed water, the increase in the damping coefficient may be due to the dynamic contact angle hysteresis generated over an oscillating period of the cantilever tip during interaction.

It is known that $\cos\theta_{adv} \leqslant \cos\theta_s \leqslant \cos\theta_{re}$, where θ_s, θ_{adv} and θ_{re} are static, advancing and receding contact angles, respectively. By advancing and receding the cantilever tip from the water surface, Tao and Bhushan (2006) measured advancing and receding contact angles for AFM probes. They reported about 20° difference of advancing and receding contact angles for silicon tips. By applying the sessile drop method on a flat silicon surface, there is also a more than 14° contact angle hysteresis (Extrand and Kumagai 1997, Tao and Bhushan 2006). Therefore, the contact angle hysteresis should be considered. To simplify the analysis, we suggest θ_c is equal to θ_{re} when the tip moves downward for each cycle of cantilever oscillation. Similarly, θ_c is equal to θ_{adv} for upward movement of the cantilever tip. Therefore, the contact angle hysteresis leads to a velocity-dependent dissipation force for each cycle of cantilever oscillation, and affects the damping coefficient.

4. Conclusions

In this study, nanobubbles were studied using tapping mode AFM on a PS coated Si wafer surface immersed in DI water. A modified liquid cell was used to improve the frequency response of AFM cantilevers in liquid. Step by step nanobubble coalescence in the same area was achieved by changing either the scan speed or scan load. The typical size of nanobubbles gradually grows from 200 nm in diameter and 20 nm in height to 690 nm and 100 nm, respectively. Results show that, in addition to scan load, scan speed can also affect nanobubble imaging. At lower scan speed, more energy will be transferred from the cantilever tip to the nanobubbles and result in nanobubble coalescence. Therefore, to get undisturbed nanobubble images, it is necessary to apply lower scan load and higher scan speed during TMAFM imaging. Nanobubble coalescence is studied. During coalescence, smaller bubbles were easier to move than bigger bubbles due to their lower interaction with sample surfaces than that of bigger

bubbles. The moved bubbles then merged into bigger ones and generated new bubbles.

Using force modulation mode, we obtain bubble height and tip–bubble adhesion information in addition to amplitude and phase shift signal. Experiments reveal that adhesion force inversely increases with the nanobubble height along nanobubble section profiles with tip–bubble interaction. This is because the tip–bubble contact area changes along section profiles. A viscoelastic model is used to analyze tip–bubble interaction. Utilizing amplitude and phase shift signals, the interaction stiffness and damping coefficient between tip and bubble can be obtained, which makes it possible to determine the mechanical properties of nanobubbles. The analytical results show that surface tension force may contribute to the attractive force presented in tip–bubble interactions. Additionally, contact angle hysteresis leads to changes in the damping coefficient in tip–bubble interactions.

Acknowledgments

Yuliang Wang acknowledges financial support from the Chinese Scholarship Council. Suggestions from Dr Xing Ling, Dr Kwang Joo Kwak and Dr Manuel L B Palacio and contact angle measurement by Yong Chae Jung are warmly acknowledged.

References

Agrawal A, Park J, Ryu D Y, Hammond P T, Russell T P and McKinley G H 2005 Controlling the location and spatial extent of nanobubbles using hydrophobically nanopatterned surfaces *Nano Lett.* **5** 1751–6

Aime J P, Boisgard R, Nony L and Couturier G 2001 Influence of noncontact dissipation in the tapping mode: attempt to extract quantitative information on the surface properties with the local force probe method *J. Chem. Phys.* **114** 4945–54

Attard P 2003 Nanobubbles and the hydrophobic attraction *Adv. Colloid Interface Sci.* **104** 75–91

Bar G, Thomann Y and Whangbo M H 1998 Characterization of the morphologies and nanostructures of blends of poly(styrene) block-poly(ethene-co-but-1-ene)-block-poly(styrene) with isotactic and atactic polypropylenes by tapping-mode atomic force microscopy *Langmuir* **14** 1219–26

Bhushan B 1999 *Principles and Applications of Tribology* (New York: Wiley) pp 314–5

Bhushan B 2002 *Introduction to Tribology* (New York: Wiley)

Bhushan B 2007 *Springer Handbook of Nanotechnology* 2nd edn (Heidelberg: Springer)

Bhushan B 2008 *Nanotribology and Nanomechanics: An Introduction* 2nd edn (Heidelberg: Springer) pp 235–74

Chen X, Davies M C, Roberts C J, Tendler S J B, Williams P M, Davies J, Dawkes A C and Edwards J C 1998 Interpretation of tapping mode atomic force microscopy data using amplitude-phase-distance measurements *Ultramicroscopy* **75** 171–81

Cottin-Bizonne C, Barentin C, Charlaix E, Bocquet L and Barrat J L 2004 Dynamics of simple liquids at heterogeneous surfaces: molecular-dynamics simulations and hydrodynamic description *Eur. Phys. J.* E **15** 427–38

Ecke S, Preuss M and Butt H J 1999 Microsphere tensiometry to measure advancing and receding contact angles on individual particles *J. Adhes. Sci. Technol.* **13** 1181–91

Extrand C W and Kumagai Y 1997 An experimental study of contact angle hysteresis *J. Colloid Interface Sci.* **191** 378–83

Garcia R and San Paulo A 1999 Attractive and repulsive tip–sample interaction regimes in tapping-mode atomic force microscopy *Phys. Rev.* B **60** 4961–7

Holmberg M, Kuhle A, Garnaes J, Morch K A and Boisen A 2003 Nanobubble trouble on gold surfaces *Langmuir* **19** 10510–3

Ishida N, Inoue T, Miyahara M and Higashitani K 2000 Nano bubbles on a hydrophobic surface in water observed by tapping-mode atomic force microscopy *Langmuir* **16** 6377–80

Ishida N, Sakamoto M, Miyahara M and Higashitani K 2002 Optical observation of gas bridging between hydrophobic surfaces in water *J. Colloid Interface Sci.* **253** 112–6

Israelachvili J 1992 *Intermolecular & Surface Forces* 3rd edn (London: Academic)

Jeffery S, Hoffmann P M, Pethica J B, Ramanujan C, Ozer H O and Oral A 2004 Direct measurement of molecular stiffness and damping in confined water layers *Phys. Rev.* B **70** 054114

Joseph P, Cottin-Bizonne C, Benoit J M, Ybert C, Journet C, Tabeling P and Bocquet L 2006 Slippage of water past superhydrophobic carbon nanotube forests in microchannels *Phys. Rev. Lett.* **97** 156104

Koishi T, Yoo S, Yasuoka K, Zeng X C, Narumi T, Susukita R, Kawai A, Furusawa H, Suenaga A, Okimoto N, Futatsugi N and Ebisuzaki T 2004 Nanoscale hydrophobic interaction and nanobubble nucleation *Phys. Rev. Lett.* **93** 185701

Lauga E and Stone H A 2003 Effective slip in pressure-driven Stokes flow *J. Fluid Mech.* **489** 55–77

Lou S T, Ouyang Z Q, Zhang Y, Li X J, Hu J, Li M Q and Yang F J 2000 Nanobubbles on solid surface imaged by atomic force microscopy *J. Vac. Sci. Technol.* B **18** 2573–5

Maali A, Cohen-Bouhacina T, Couturier G and Aime J P 2006a Oscillatory dissipation of a simple confined liquid *Phys. Rev. Lett.* **96** 086105

Maali A, Hurth C, Cohen-Bouhacina T, Couturier G and Aime J P 2006b Improved acoustic excitation of atomic force microscope cantilevers in liquids *Appl. Phys. Lett.* **88** 163504

Ou J, Perot B and Rothstein J P 2004 Laminar drag reduction in microchannels using ultrahydrophobic surfaces *Phys. Fluids* **16** 4635–43

Paulo A S and Garcia R 2002 Unifying theory of tapping-mode atomic-force microscopy *Phys. Rev.* B **66** 041406

Sbragaglia M and Prosperetti A 2007 Effective velocity boundary condition at a mixed slip surface *J. Fluid Mech.* **578** 435–51

Scheludko A D and Nikolov A D 1975 Measurement of surface-tension by pulling a sphere from a liquid *Colloid Polym. Sci.* **253** 396–403

Simonsen A C, Hansen P L and Klosgen B 2004 Nanobubbles give evidence of incomplete wetting at a hydrophobic interface *J. Colloid Interface Sci.* **273** 291–9

Steinberger A, Cottin-Bizonne C, Kleimann P and Charlaix E 2007 High friction on a bubble mattress *Nat. Mater.* **6** 665–8

Steitz R, Gutberlet T, Hauss T, Klosgen B, Krastev R, Schemmel S, Simonsen A C and Findenegg G H 2003 Nanobubbles and their precursor layer at the interface of water against a hydrophobic substrate *Langmuir* **19** 2409–18

Switkes M and Ruberti J W 2004 Rapid cryofixation/freeze fracture for the study of nanobubbles at solid–liquid interfaces *Appl. Phys. Lett.* **84** 4759–61

Tamayo J and Garcia R 1996 Deformation, contact time, and phase contrast in tapping mode scanning force microscopy *Langmuir* **12** 4430–5

Tao Z H and Bhushan B 2006 Wetting properties of AFM probes by means of contact angle measurement *J. Phys. D: Appl. Phys.* **39** 3858–62

Tyrrell J W G and Attard P 2002 Atomic force microscope images of nanobubbles on a hydrophobic surface and corresponding force-separation data *Langmuir* **18** 160–7

Vinckier A, Dumortier C, Engelborghs Y and Hellemans L 1996 Dynamical and mechanical study of immobilized microtubules

with atomic force microscopy *J. Vac. Sci. Technol.* B **14** 1427–31

Vinogradova O I, Butt H J, Yakubov G E and Feuillebois F 2001 Dynamic effects on force measurements. I. Viscous drag on the atomic force microscope cantilever *Rev. Sci. Instrum.* **72** 2330–9

Watts E T, Krim J and Widom A 1990 Experimental observation of interfacial slippage at the boundary of molecularly thin films with gold substrates *Phys. Rev.* B **41** 3466–72

Yang J W, Duan J M, Fornasiero D and Ralston J 2003 Very small bubble formation at the solid–water interface *J. Phys. Chem.* B **107** 6139–47

Zhang X H, Maeda N and Craig V S J 2006 Physical properties of nanobubbles on hydrophobic surfaces in water and aqueous solutions *Langmuir* **22** 5025–35

Zhong Q, Inniss D, Kjoller K and Elings V B 1993 Fractured polymer silica fiber surface studied by tapping mode atomic-force microscopy *Surf. Sci.* **290** L688–92